Muonic X-ray intensities in phosphorus- and selenium modifications

Autor(en): **Kaeser, K. / Dubler, T. / Robert-Tissot, B.**

Objekttyp: **Article**

Zeitschrift: **Helvetica Physica Acta**

Band (Jahr): **52 (1979)**

Heft 2

PDF erstellt am: **26.04.2024**

Persistenter Link: https://doi.org/10.5169/seals-115029

Helvetica Physica Acta, Vol. 52 (1979), Birkhäuser Verlag, Basel

Muonic X-ray intensities in phosphorus- and selenium modifications[1])

by **K. Kaeser, T. Dubler, B. Robert-Tissot, L. A. Schaller, L. Schellenberg** and **H. Schneuwly**

Institut de Physique de l'Université CH-1700 Fribourg, Switzerland

(3. IV. 1979)

Abstract. Muonic X-ray intensity measurements have been performed at SIN on allotropic modifications of phosphorus (white, red and black) and of selenium (red and black). Structure effects have been found in the intensity ratios of the K-series between amorphous and crystalline modifications of the same element. The effect in the higher series (*Se*) is less pronounced. On the other hand, the two crystalline phosphorus modifications (red and black) show the same intensity behavior.

The root-mean-square radii $\langle r^2\rangle^{1/2}$ of phosphorus and (natural) selenium were found to be 3.187(3) fm and 4.138(1) fm respectively.

1. Introduction

Even if a lot of experimental and theoretical work has been accomplished during the recent years on the atomic capture of negatively charged exotic particles, the formation mechanism of exotic atoms remains an unsolved question ([1] and references cited therein). Nevertheless, experimental results and theoretical calculations seem to establish that the atomic capture of muons and mesons proceeds predominantly through Auger electron ejection and that, in comparison, the radiative capture is almost negligible. This allows *a priori* an influence of the chemical structure of matter on the Coulomb capture mechanism of exotic particles. From the experimental results of Wiegand and Godfrey [2] in kaonic atoms e.g., a correlation can be established between the radiative intensities of circular orbit transitions and the interatomic distances [3, 4]. A similar correlation exists with the electron densities in the outer part of the host atom [5]. Correlations between the muonic cascade intensity pattern and the formal valence state are also possible [6, 7, 8]. In addition, muonic capture rates are influenced by the formal valence state of elements in compounds [9].

Similar correlations are expected if the muonic atom is embedded in different solid state structures. The only measurement which showed a solid state effect has been performed in selenium [10]. The ratio of the intensity ratios $I(5\rightarrow 3)/I(4\rightarrow 3)$ between red and black selenium was found to be 0.74 ± 0.06. In the same paper, the corresponding intensity ratio for pionic X-rays was found to be compatible with unity (1.02 ± 0.04). It is not evident that the capture mechanism

[1]) Partly supported by the Swiss National Science Foundation.

should be different between pions and muons [1, 11]. Knight et al. [12] have investigated the carbon muonic X-ray intensities in diamond and graphite. They found no significant differences, although the two allotropic states of carbon differ both in the interatomic distances and in the chemical bond. The same authors [12] studied also the muonic X-ray intensity pattern of boron nitride in the graphite and the diamond modifications. Again, no significant difference was found with the exception of the $I(6\rightarrow 1)/(2\rightarrow 1)$ intensity ratio in nitrogen. The same negative result holds for the oxygen muonic Lyman series in water and ice [12]. Hence, one may ask whether solid state modifications influence at all the muonic capture mechanism or whether their effect is so small that it cannot be detected. In order to shed light on such questions, we have measured the muonic cascade intensities in the three modifications of phosphorus (white, red and black) and the two modifications of selenium (red and black). A similar study has recently been made by Zinov et al. [13] on the red and white phosphorus modifications which will be discussed in Section 5.3.1.

2. Targets

2.1. *Allotropy of phosphorus* [14]

White phosphorus is a translucent, soft and phosphorescent substance in air. It has a density of 1.82 g/cm^3, melts at 44.1°C and boils at 280.5°C. Its structure is supposed to be that of a solidified vapor [15], i.e. a stochastic conglomerate of P_4-tetrahedrons whose sides are 2.21 Å long. Because of the amorphous structure, white phosphorus is chemically very reactive (therefore very poisonous) and easily soluble in solvents like carbon disulfide, chlorosulfonic acid and phosphorus trichloride.

Red phosphorus is obtained from the thermodynamically less stable white phosphorus by heating above 180°C. As a result of linear polymerisation of the atoms, it consists of long chains, which are irregularly screw cross-linked [16]. In this structure, phosphorus has a density of 2.16 g/cm^3 and a low chemical reactivity (and is thus not poisonous). It is completely unsoluble in solvents.

Black phosphorus is considered as the metallic modification of phosphorus, since it appears as an iron-grey, metallic-brilliant rhombic crystal and has a relatively high conductivity combined with a rectifying effect. It is produced from white phosphorus at temperatures of about 400°C under pressure and through the catalytic action of metallic mercury [17]. As a result of the pressure and the stereospecific influence of the catalyst, the intermediately formed polymer chains approach each other, so that the third valencies of the phosphorus atoms can saturate with atoms of lower-lying chains. Thus, double layers of parallel chains with a layer distance of 3.68 Å are formed. Black phosphorus has a density of 2.69 g/cm^3. At room temperature, it is the thermodynamically most stable modification of phosphorus.

2.2 *Allotropy of selenium*

Red selenium is the thermodynamically less stable amorphous modification. From the crystal-optical point of view, it is identical with the liquid melt.

Presumably, red selenium is a conglomerate of Se_8-rings with a density of 4.26 g/cm^3.

Black selenium is obtained from the red modification by tempering at 100–200°C. Its structure can be considered as an arrangement of helically wound chain molecules held together by Van der Waals forces [18]. The structure element has a repetition length of 4.959 Å, a distance between the chains of 4.364 Å and an interatomic distance within the chain of 2.32 Å [19]. As metallic modification, black selenium has a relatively good conductivity when irradiated by light. Its density is 4.80 g/cm^3.

2.3. *Preparation of the targets*

The targets were flat discs of 7.4 cm diameter and 0.6–0.7 cm thickness, depending on the packing density. These disks were packed into a thin ring of plexiglass covered on both sides by a thin mylar foil. The thicknesses in beam direction were 1.732 g/cm^2 for all three phosphorus targets, 0.821 g/cm^2 for red selenium and 1.185 g/cm^2 for the black selenium modification.

The targets have been prepared in the following way: The white phosphorus of quality DAB 6 had been submitted to a stream distillation (under protective gas) in order to eliminate arsenic impurities [20]. After that, the high purity phosphorus was formed under water to the target dimensions then dried and packed under a protective gas cover. The red and black phosphorus powders of commercial quality of at least 96% purity were pressed to the target dimensions.

The red selenium had to be prepared just before the start of the measurements, because it transforms already at room temperature to the black modification. Black selenium of 99.95% purity was dissolved at 150–200°C in concentrated sulfuric acid, then hotly filtrated. The cooled filtrate was isothermically diluted so that freshly precipitating red selenium was obtained. The powder was dried at room temperature in vacuum, pressed to the target dimensions and packed and stored in a refrigerator.

The black selenium of commercial quality (99.95% purity) was first tempered during two days under protective gas at approximately 180°C in order to convert eventual traces of red selenium into the black modification. Afterwards, this powdery black selenium was pressed like the other targets.

3. Experimental set-up

The measurements were performed at the μEl-channel of the 590 MeV proton accelerator of the Swiss Institute for Nuclear Research (SIN) in Villigen. Pions of 150 MeV/c momentum, extracted from the beryllium production target, decayed in a superconducting solenoid of 7 m length into muons. Muons of 85 MeV/c momentum from backward-decaying pions were guided to the experimental area, where the target was placed in the beam focus of 6×6 cm^2. A conventional telescope [21] consisting of four scintillation counters and a beryllium degrader were used in order to define the stopped muons in the target.

The muonic X-rays were measured with two germanium detectors, both placed in the target plane perpendicular to the beam. For phosphorus, a 2.2 cm^3 planar and a 50 cm^3 coaxial Ge(Li)-diode were employed. For selenium, the

smaller detector was replaced by a 2.4 cm^3 intrinsic Ge-diode. Typical in-beam energy resolutions for the detectors were: 2.4 keV for the 50 cm^3 detector at 1332 keV, 0.70 keV for the 2.4 cm^3 diode and 0.75 keV for the 2.2 cm^3 detector at 122 keV.

The pulse heights of the signals registered by the two detectors were analyzed using 8192 channel ADC's (LABEN 8215). Prompt and delayed events with respect to a muon stop as well as energy calibration events were stored on magnetic tape using a CAMAC-PDP 11/40 system. Events occurring within a time window of 20 ns after the muon stop signal were considered as prompt events. Detector signals registered in a time window of 20 to 250 ns after the muon stop signal were stored as delayed events. Signals occurring after delayed events until a new muon stop were interpreted as calibration signals. The spectra were reconstructed and analyzed on the IBM 370 computer of the University of Fribourg. More details about the electronic setup may be found in Ref. [21].

Typical stop rates were of the order of 500 kHz for a proton current of 20 μA. Typical counting rates were 6 kHz in the 50 cm^3 diode and 3 kHz in the small detectors. The analyzed spectra were collected each in about 5 hours beamtime.

4. Data analysis

4.1. *Analysis of the spectra*

For each target, six 8192 channel spectra were obtained. They were analyzed using the computer code LINFIT as described in Refs. [21, 22]. If more than one muonic X-ray transition was present in the fit interval, the parameters of each peak, i.e. position, width and intensity, were determined independently as long as the separation between neighbouring lines was greater than about 40% of the line width. Special care was taken with background lines such as delayed γ-rays and muonic X-rays from possible target contaminations and from the environment which could otherwise falsify the intensities of the interesting muonic X-rays. Delayed line intensities in the prompt spectra could be estimated from the delayed spectra. Muonic background X-rays, especially from the carbon and oxygen in the scintillators, the plexiglass ring with the mylar cover and the nitrogen and oxygen in the air could be evaluated from the intensities of other members of the respective Lyman series.

4.2. *Self-absorption in the target*

The absorption of the muonic X-rays of interest within the target was calculated using the computer code ABSORB [23]. There, the intensities emitted from a given point within the target are determined taking beam and target geometry and muon stop density distribution in the target into account. The absorption in the direction of the detector is calculated for each point of the target, employing for the energies of interest the absorption coefficients of Storm and Israel [24]. By integrating over the whole target volume, an average absorption factor as a function of energy is obtained.

4.3. *Detector efficiencies*

The energy dependence of the photopeak efficiency was measured for each detector before and after the muonic X-ray measurements using a similar electronic set-up. The intensity calibration sources were a set of Saclay BNM sources. Figure 1 shows measured efficiencies for the 50 cm^3 and the 2.4 cm^3 Ge diodes.

The function used to approximate the measured energy dependent efficiency $\varepsilon(E)$ was that of Winiger et al. [25] (solid curves in Fig. 1).

$$\varepsilon(E)=\tfrac{1}{2}\cdot\varepsilon(E_0)\cdot\left[\left(\frac{E}{E_0}\right)^{\alpha}+\left(\frac{E}{E_0}\right)^{\beta}\right]\cdot[1-\exp(\gamma E)]^{\delta}$$

In this formula, $\varepsilon(E_0)$ is the efficiency at the reference energy E_0, and α, β, γ and δ are adjustable parameters.

4.4 *Relative transition intensities in muonic phosphorus*

In fitting the intensities of the different series, the following procedure has been employed. For the Lyman series, the $2p\rightarrow 1s$ up to the $8p\rightarrow 1s$ transitions have been analyzed independently from each other. Position and width of the fine structure components have been correlated. The $9p\rightarrow 1s$ up to the $14p\rightarrow 1s$ transitions could not be resolved experimentally and have therefore been correlated in energy, width and intensity in order to obtain a good fit of the upper end of the Lyman series.

The line intensities of the Balmer series up to the $8d\rightarrow 2p$ transitions were determined by correlating width and position of the fine structure components. In

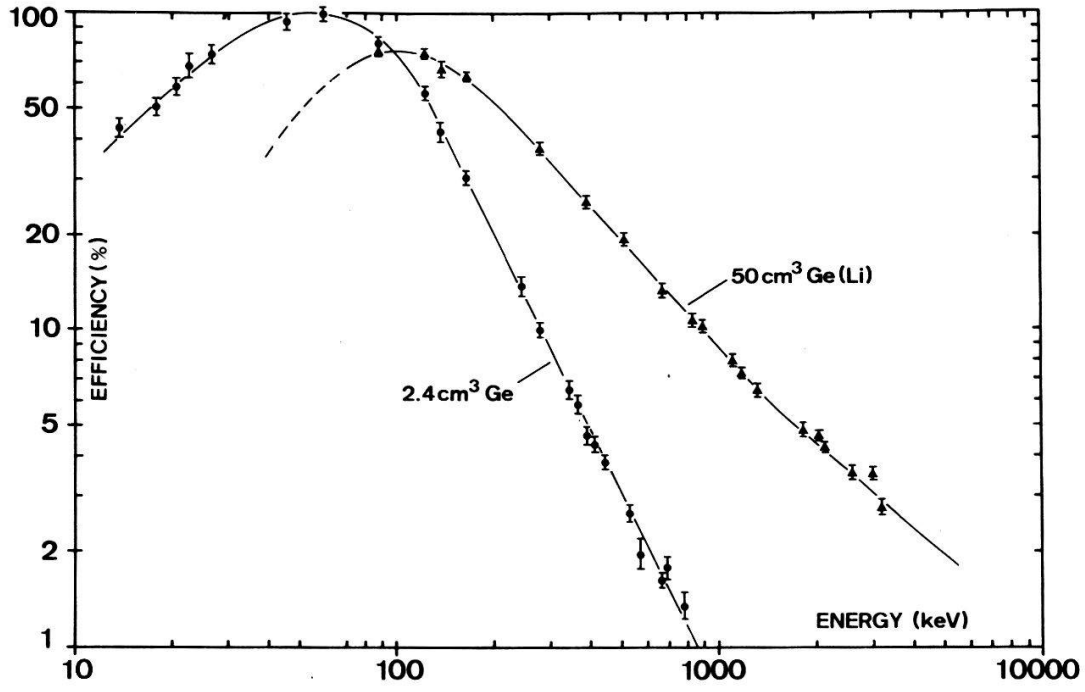

Figure 1
Photopeak efficiencies as a function of γ-energy. The curves represent the best fits using the formula in Section 4.3. The corresponding regression-parameters for the 50 cm^3 (2.4 cm^3) diode are $E_0=$ 480.85 (661.6) keV, $\varepsilon(E_0)=0.2013$ (0.03232), $\alpha=-1.5663$ (−2.1621), $\beta=-0.7653$ (−∞), $\gamma=$ −0.01961 (−0.02562) keV^{-1} and $\delta=4.4858$ (4.3113).

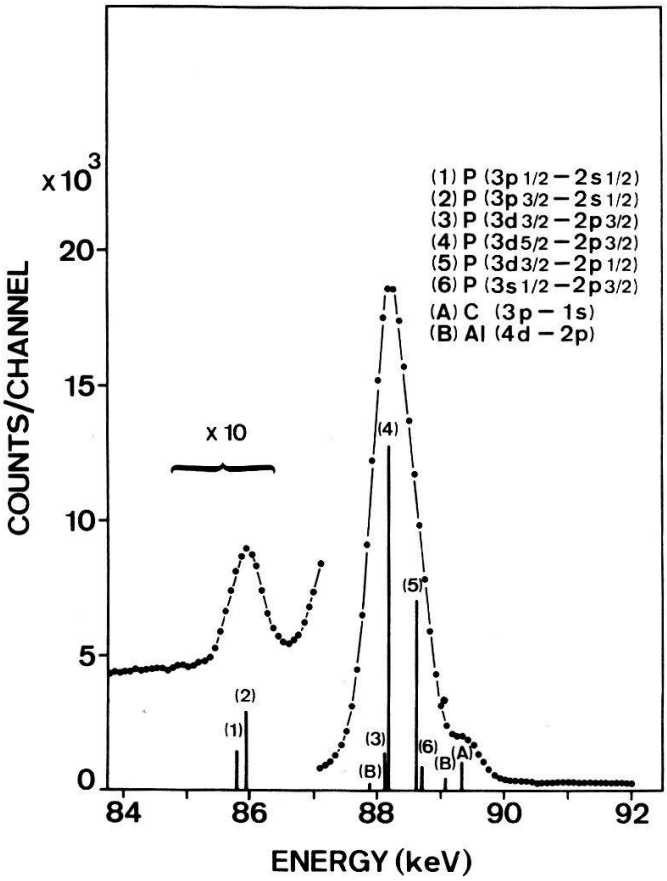

Figure 2
μ^-P(3→2) line structure including the background transitions μ^-C(3→1) and μ^-Al(4→2).

this way, an exact analysis of the $5d \rightarrow 2p$ transitions in presence of the $2p \rightarrow 1s$ muonic oxygen X-ray, due to the oxygen present in the target assembly and the surroundings, has been achieved, although the energy difference between the μ^-P $(5d_{5/2} \rightarrow 2p_{3/2})$ and the μ^-O$(3p_{3/2} \rightarrow 1s_{1/2})$ lines is only 590 eV. A similar problem exists in the analysis of the μ^-P(3→2) transitions at 88.5 keV (Fig. 2). Here, the μ^-Al(4→2) and the μ^-C(3→1) transitions originating from stopped muons in the target holder and the telescope counters are not resolved from the components of the μ^-P(3→2) transitions. The intensities of these background lines could be determined by using the experimentally measured intensities of the μ^-Al(3→2), μ^-Al(5→2), μ^-C(2→1) and μ^-C(4→1) transitions and the corresponding intensity ratios from the selenium runs.

Hyperfine splittings due to the quadrupole moment of the phosphorus nucleus have been neglected in the analysis, since the splitting in the μ^-P$(3d \rightarrow 2p)$ transitions is of the order of only 60 eV.

4.5 *Relative transition intensities in muonic selenium*

The general procedure was the same as in the case of phosphorus. Due to the higher Z value of selenium, the fine structure components of the μ^-Se(2→1) and μ^-Se(3→1) lines were sufficiently separated to be determined independently from each other. For the higher transitions, where the fine structure splittings become less than 40% of the line width, the components were correlated as in the case of phosphorus.

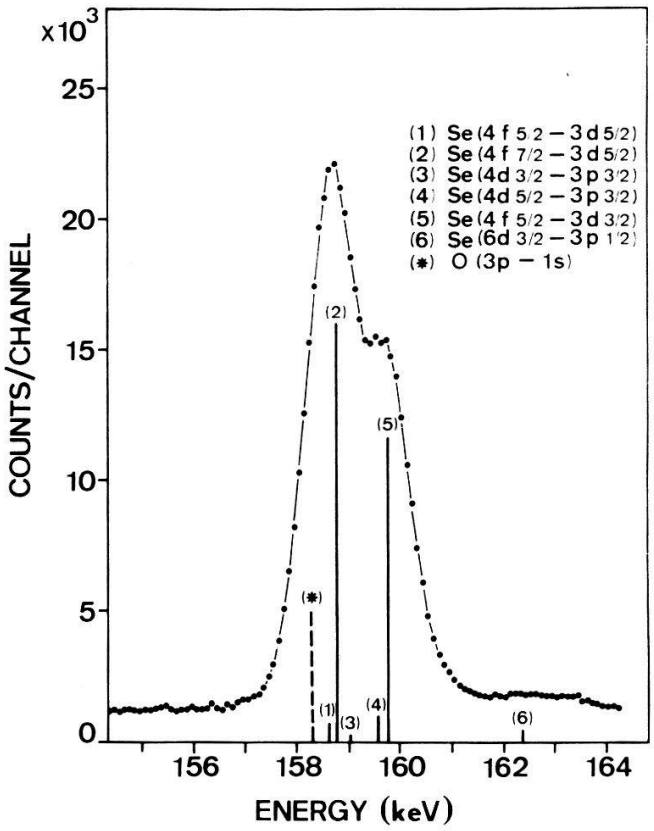

Figure 3
μ^-Se (4→3) line structure including the background transition μ^-O(3→1).

Special care has been taken in order to separate the μ^-O(3→1) background line from the μ^-Se(4→3) transitions (Fig. 3). The energy difference between the oxygen line and the μ^-Se($4f_{7/2}\rightarrow 3d_{5/2}$) line is less than 40% of the line width. As a fact, the oxygen background was considerably higher in red selenium than in the black modification, since red selenium easily adsorbs water. An interpolation of the μ^-O(3→1) intensity from the fitted μ^-O(2→1) and μ^-O(4→1) intensities by employing intensity ratios measured in other oxygen containing compounds is a first estimate. However, the relative intensities of the oxygen Lyman series can be different, if the oxygen is differently bound in a molecule [6]. By correlating energywise the μ^-O(3→1) line to the μ^-Se(4→3) lines and by using as a starting parameter for the μ^-O(3→1) intensity the interpolation as described above, intensities of both transitions could be determined. The relative intensities obtained for the oxygen Lyman series turned out to be in good agreement with recent experimental results [26] for water.

5. Results

5.1 *Transition energies in phosphorus and selenium*

The energies of the measured muonic X-rays have been calibrated employing a similar procedure as the one described in the paper by Dubler et al. [21]. The calibration sources in the case of phosphorus were ^{137}Cs and ^{192}Ir. For selenium, we used in addition ^{24}Na and ^{56}Co. The energy range of interest could be

accurately fitted with a parabola. Table 1 shows the measured energies of the muonic X-rays in selenium and phosphorus.

Table 1 contains only energies of transitions which were fitted independently of other lines. Not listed fine structure components were correlated with respect to energy and intensity to the main component of the transition. From the measured transition energies of the Lyman series, which are sensitive to the nuclear charge distribution, one parameter of this distribution was calculated using the computer code MUON [27]. Fixing the Fermi skin thickness parameter t at 2.30 fm, the half density parameter c was determined to be 3.258(4) fm for

Table 1
Energies of transitions in muonic phosphorus and selenium

Transition	Phosphorus (red) energy (keV)	Selenium (red) energy (keV)
$5g_{9/2}\rightarrow 4f_{7/2}$		73.429 (50)
$6g_{9/2}\rightarrow 4f_{7/2}$		113.055 (55)
$7g_{9/2}\rightarrow 4f_{7/2}$		137.211 (70)
$8g_{9/2}\rightarrow 4f_{7/2}$		152.710 (100)
$4f_{7/2}\rightarrow 3d_{5/2}$		158.871 (30)
$5f_{7/2}\rightarrow 3d_{5/2}$		232.119 (30)
$6f_{7/2}\rightarrow 3d_{5/2}$		271.892 (50)
$7f_{7/2}\rightarrow 3d_{5/2}$		295.611 (90)
$8f_{7/2}\rightarrow 3d_{5/2}$		311.187 (120)
$3p_{3/2}\rightarrow 2s_{1/2}$	85.804 (60)	394.007 (100)
$3d_{5/2}\rightarrow 2p_{3/2}$	88.007 (50)	455.388 (30)
$3d_{3/2}\rightarrow 2p_{1/2}$		465.629 (30)
$3s_{1/2}\rightarrow 2p_{3/2}$	88.315 (80)	
$4p_{3/2}\rightarrow 2s_{1/2}$	116.594 (70)	
$4d_{5/2}\rightarrow 2p_{3/2}$	118.749 (60)	614.023 (100)
$4d_{3/2}\rightarrow 2p_{1/2}$	119.174 (60)	624.960 (70)
$5p_{3/2}\rightarrow 2s_{1/2}$	130.852 (70)	
$5d_{5/2}\rightarrow 2p_{3/2}$	132.948 (60)	687.234 (50)
$5d_{3/2}\rightarrow 2p_{1/2}$	133.237 (60)	698.526 (50)
$6p_{3/2}\rightarrow 2s_{1/2}$	138.585 (75)	
$6d_{5/2}\rightarrow 2p_{3/2}$	140.800 (65)	727.106 (85)
$6d_{3/2}\rightarrow 2p_{1/2}$	140.926 (65)	738.537 (85)
$7d_{5/2}\rightarrow 2p_{3/2}$	145.330 (70)	751.102 (100)
$7d_{3/2}\rightarrow 2p_{1/2}$		762.348 (100)
$8d_{5/2}\rightarrow 2p_{3/2}$	148.310 (70)	766.509 (120)
$8d_{3/2}\rightarrow 2p_{1/2}$		777.136 (120)
$9d_{5/2}\rightarrow 2p_{3/2}$		777.971 (140)
$10d_{5/2}\rightarrow 2p_{3/2}$		784.774 (160)
$11d_{5/2}\rightarrow 2p_{3/2}$		790.389 (190)
$2p_{1/2}\rightarrow 1s_{1/2}$		1946.785 (80)
$2p_{3/2}\rightarrow 1s_{1/2}$	456.985 (20)	1958.354 (80)
$3p_{3/2}\rightarrow 1s_{1/2}$	544.960 (20)	2412.590 (160)
$4p_{3/2}\rightarrow 1s_{1/2}$	575.689 (25)	2572.100 (300)
$5p_{3/2}\rightarrow 1s_{1/2}$	589.861 (30)	2645.872 (350)
$6p_{3/2}\rightarrow 1s_{1/2}$	597.607 (30)	2685.645 (400)
$7p_{3/2}\rightarrow 1s_{1/2}$	602.267 (50)	2709.278 (470)
$8p_{3/2}\rightarrow 1s_{1/2}$	605.218 (55)	2724.899 (520)

phosphorus and 4.715(1) fm for selenium (natural isotope mixture). The respective root-mean-square radii $\langle r^2 \rangle$ for the two elements are 3.187(3) fm and 4.138(1) fm. The results for phosphorus (^{31}P) have already been published [28].

The precision of the energies is determined by the precision of the calibration sources and the statistical uncertainty of the line positions. In some cases, systematic energy shifts of ≤ 15 eV between the calibration spectra and the prompt spectra had to be taken into account.

5.2. *Absolute cascade intensities*

The absolute intensities of the muonic cascade transitions were determined by adding the respective peaks of the prompt and the delayed spectra. The intensities of the prompt X-rays appearing in the delayed spectra were of the order of 10%. The intensities were corrected for self-absorption in the target and detector efficiency. The final intensities are listed in Tables 2 and 3. They are normalized to the sum of the radiation intensities of the Lyman series transitions, which was taken to be 100%. The relative intensities of all transitions between $9 \rightarrow 1$ to $14 \rightarrow 1$ were correlated according to the results of the cascade intensity code CASC1 [29], which starts with a statistical population at $n = 20$. The intensities of the transitions from $15 \rightarrow 1$ to $20 \rightarrow 1$ were taken directly from the calculation and used in the normalization. The uncertainty in the normalization using such estimates should not exceed 0.8%.

The errors of the absolute cascade intensities given in Tables 2 and 3 are combined errors of the statistical uncertainty (fit errors) and the uncertainties in the self-absorption correction and the detector efficiency calibration. For circular transitions, the statistical errors are negligible compared to the errors in the detector efficiencies, whereas for transitions near the limit of a series (high Δn), the opposite is true. For low energy transitions, i.e. below 100 keV, the self-absorption became important. For example, the target transmission was only 39% for the μ^-Se($6 \rightarrow 5$) transition at 39.8 keV. Since the uncertainty in the self-absorption correction may be as high as 10%, the intensities of the Pfund series

Table 2
Experimental intensities of muonic phosphorus

	Transition	Energy (keV)	Intensities (%) of White phosphorus	Red phosphorus	Black phosphorus
Lyman-series	$2 \rightarrow 1$	457.0	76.6 ±1.9	75.2 ±1.9	75.2 ±1.9
	$3 \rightarrow 1$	545.0	7.04 ±0.19	7.25 ±0.19	7.14 ±2.0
	$4 \rightarrow 1$	575.7	3.74 ±0.11	4.04 ±0.11	4.00 ±0.11
	$5 \rightarrow 1$	589.9	3.52 ±0.11	3.85 ±0.11	3.78 ±0.12
	$6 \rightarrow 1$	597.6	2.45 ±0.08	2.74 ±0.08	2.69 ±0.08
	$7 \rightarrow 1$	602.3	1.31 ±0.04	1.49 ±0.04	1.47 ±0.04
	$8 \rightarrow 1$	605.2	0.395±0.02	0.439±0.02	0.475±0.02
Balmer-series	$3 \rightarrow 2$	88.0	57.9 ±3.3	54.5 ±3.3	54.9 ±3.4
	$4 \rightarrow 2$	118.7	11.17 ±0.31	10.81 ±0.31	11.10 ±0.32
	$5 \rightarrow 2$	132.9	4.43 ±0.23	4.67 ±0.23	4.32 ±0.23
	$6 \rightarrow 2$	140.8	2.70 ±0.10	2.62 ±0.10	2.62 ±0.10
	$7 \rightarrow 2$	145.3	1.21 ±0.04	1.20 ±0.04	1.27 ±0.04
	$8 \rightarrow 2$	148.3	0.331±0.02	0.297±0.02	0.327±0.02

Table 3
Experimental intensities of selenium

	Transition	Energy (keV)	Intensities (%) of Red selenium	Black selenium
Lyman-series	2→1	1955	86.2 ±2.5	86.2 ±2.5
	3→1	2411	5.97±0.26	5.81±0.33
	4→1	2572	1.12±0.13	1.20±0.15
	5→1	2646	0.91±0.12	0.87±0.13
	6→1	2685	0.64±0.10	0.51±0.11
	7→1	2709	0.59±0.07	0.78±0.09
	8→1	2724	0.41±0.06	0.66±0.08
	$\sum(9\div15)\rightarrow1$		2.90±0.20	3.38±0.26
Balmer-	3→2	455	68.2 ±2.0	68.8 ±2.0
	4→2	614	9.71±0.31	9.77±0.34
	5→2	687	2.76±0.13	2.58±0.15
	6→2	727	1.67±0.09	1.61±0.12
	7→2	751	1.16±0.08	1.21±0.10
	8→2	766	0.77±0.09	0.69±0.10
	9→2	777	0.64±0.08	0.56±0.09
	10→2	784	0.43±0.05	0.27±0.05
	11→2	790	0.24±0.04	0.17±0.05
Paschen-	4→3	158.9	58.3 ±1.7	54.7 ±1.6
	5→3	232.1	10.04±0.32	9.57±0.30
	6→3	271.9	4.26±0.25	3.94±0.16
	7→3	295.6	2.80±0.13	2.88±0.14
	8→3	311.2	0.84±0.05	0.86±0.05
Brackett-	5→4	73.4	38.5 ±1.1	33.8 ±1.1
	6→4	113.1	10.11±0.29	9.27±0.34
	7→4	137.2	4.01±0.14	3.45±0.12
	8→4	152.7	1.38±0.08	1.16±0.07

in muonic selenium are not given in the tables. The same argument holds for the Paschen series in phosphorus.

Using the cascade intensity code CASC1 [29], but employing Ferrell's formula [33] for the electron conversion, an attempt has been made to reproduce the measured muonic intensities in phosphorus and selenium. The initial capture level was assumed to be $n = 14$ [22]. Varying the parameter α of a modified statistical population distribution $P(l) \sim (2l+1) \cdot \exp(\alpha l)$ over the angular momentum states l, a value for α corresponding to the minimum χ^2-fit can be obtained. The results for selenium are given in Section 5.3.2 for the two modifications. In the case of phosphorus, no satisfactory fits could be obtained using such a modified statistical population. We have not pursued further this comparison by varying other parameters, because we plan to use the recently published more sophisticated cascade code MUONOO [30] to examine initial capture distributions in a more general frame.

5.3 *Relative intensity ratios*

In order to see whether the initial capture distribution and the subsequent cascade of the muon are affected by the allotropy of the investigated element, the

Table 4
Relative muonic intensity ratios of Lyman-series in phosphorus

$\frac{n\to1}{2\to1}$	P $\left(\frac{\text{Black}}{\text{Red}}\right)$	P $\left(\frac{\text{White}}{\text{Red}}\right)$	P $\left(\frac{\text{White}}{\text{Black}}\right)$
$n=2$	1	1	1
$n=3$	0.985±2.2%	0.954±2.2%	0.969±2.2%
$n=4$	0.989±2.4%	0.910±2.4%	0.920±2.4%
$n=5$	0.983±2.5%	0.898±2.6%	0.913±2.6%
$n=6$	0.980±2.6%	0.876±2.7%	0.894±2.7%
$n=7$	0.985±3.0%	0.864±3.1%	0.877±3.1%
$n=8$	1.083±7.5%	0.885±7.8%	0.817±7.7%

Relative muonic intensity ratios of Balmer-series in phosphorus

$\frac{n\to2}{3\to2}$	P $\left(\frac{\text{Black}}{\text{Red}}\right)$	P $\left(\frac{\text{White}}{\text{Red}}\right)$	P $\left(\frac{\text{White}}{\text{Black}}\right)$
$n=3$	1	1	1
$n=4$	1.020±3.4%	0.973±2.5%	0.954±3.0%
$n=5$	0.918±5.0%	0.893±4.8%	0.973±4.9%
$n=6$	0.994±4.4%	0.972±5.3%	0.978±4.9%
$n=7$	1.050±2.6%	0.948±2.7%	0.902±2.7%
$n=8$	1.092±6.3%	1.050±6.9%	0.962±6.6%

respective intensities have to be compared. If ratios of intensity ratios with respect to the series heads are taken, the errors are only due to fit uncertainties, because errors due to detector efficiency, calibration and self-absorption cancel. The relative intensity ratios between the three modifications of phosphorus are given in Table 4. For the two selenium modifications, the results are shown in Table 5.

5.3.1. *Phosphorus*

The relative intensity ratios between the three phosphorus targets are graphically displayed in Fig. 4. These diagrams illustrate that there is no difference in

Table 5
Relative muonic intensity ratios of red to black selenium

n	Lyman-series Se $\left(\frac{n\to1}{2\to1}\right)$	Balmer-series Se $\left(\frac{n\to2}{3\to2}\right)$	Paschen-series Se $\left(\frac{n\to3}{4\to3}\right)$	Brackett-series Se $\left(\frac{n\to4}{5\to4}\right)$	Band-heads Se $\left(\frac{n\to(n-1)}{2\to1}\right)$
2	1				1
3	1.026±6.0%	1			0.989±5.8%
4	0.937±17.0%	1.002±2.6%	1		1.062±6.5%
5	1.048±20.0%	1.078±6.3%	0.986±1.9%	1	1.137±7.0%
6	1.237±26.0%	1.044±8.2%	1.017±4.1%	0.957±1.0%	
7	0.758±16.0%	0.969±10%	0.913±5.6%	1.022±2.6%	
8	0.624±19.0%	1.126±18.0%	0.913±6.9%	1.049±7.0%	
9		1.140±20.0%			
10		1.574±21.0%			
11		1.429±32.0%			

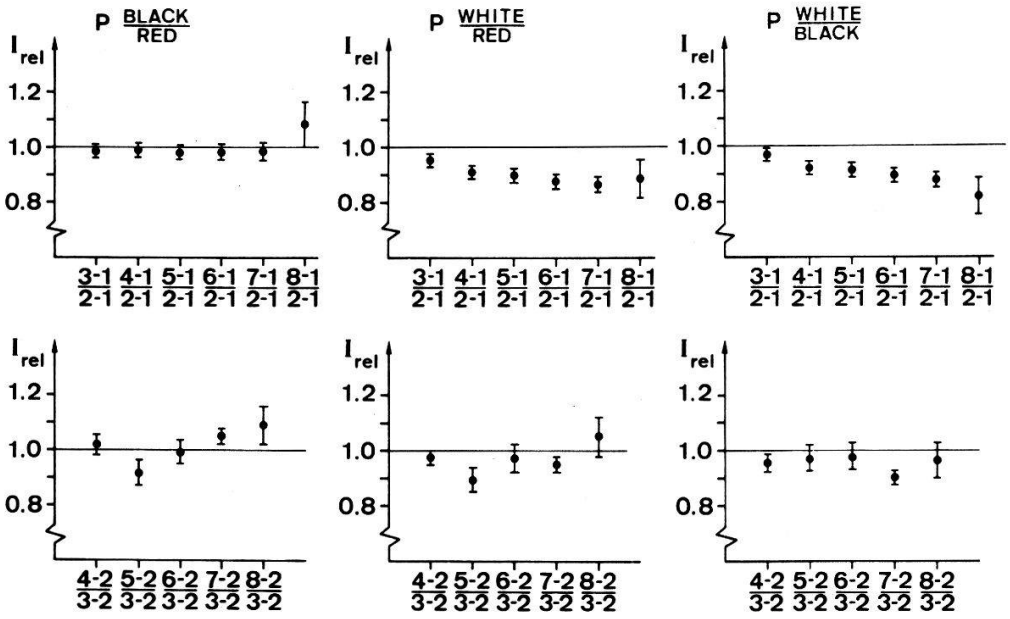

Figure 4
Relative muonic intensity ratios for the three phosphorus modifications white, red and black.

the relative muonic X-ray intensities of the Lyman series between the black (b) and the red (r) modification. However, a net difference appears between the white (w) and the red phosphorus and therefore also between the white and the black modification. The intensities of the higher Lyman series transitions relative to the $\mu^- P(2\rightarrow 1)$ intensity in white phosphorus decrease significantly with increasing principal quantum number n as compared to the red and the black modifications. The relative intensity ratios between two modifications can be represented in a linear form:

$$\left.\frac{I(n\rightarrow 1)}{I(2\rightarrow 1)}\right|_b : \left.\frac{I(n\rightarrow 1)}{I(2\rightarrow 1)}\right|_r = (1.000\pm 0.005) - (3.2\pm 2.4)\cdot 10^{-3}\cdot (n-2)$$

$$\left.\frac{I(n\rightarrow 1)}{I(2\rightarrow 1)}\right|_w : \left.\frac{I(n\rightarrow 1)}{I(2\rightarrow 1)}\right|_r = (1.000\pm 0.006) - (30.9\pm 2.9)\cdot 10^{-3}\cdot (n-2)$$

$$\left.\frac{I(n\rightarrow 1)}{I(2\rightarrow 1)}\right|_w : \left.\frac{I(n\rightarrow 1)}{I(2\rightarrow 1)}\right|_b = (1.000\pm 0.004) - (27.9\pm 1.9)\cdot 10^{-3}\cdot (n-2)$$

In this representation, a non-vanishing slope is an indication for a (systematical) structure effect. In the first intensity ratios the slope is comparable to its uncertainty, i.e. no systematic difference is measured. The intensity ratios white/red and white/black resp. have slopes which are 10 to 15 times greater than their corresponding uncertainties. They show therefore significant systematic structure effects. This finding is in good agreement with a recent, but three times less accurate measurement [13] of the same white-to-red phosphorus ratio.

The same structure effect should appear in the $(np\rightarrow 2s)$ series. However, due to the high statistical uncertainty of these weak transitions, no significant deviations from unity could be found in the corresponding $(np\rightarrow 2s)$ intensity ratios.

5.3.2. *Selenium*

The relative intensity ratios between the red (r) and the black (b) modifications are shown in Fig. 5.

Again employing a linear regression curve, one obtains for the Lyman-, Balmer- and bandhead-series:

$$\left.\frac{I(n\to 1)}{I(2\to 1)}\right|_r : \left.\frac{I(n\to 1)}{I(2\to 1)}\right|_b = (1.000\pm 0.028) - (44\pm 14)\cdot 10^{-3}\cdot (n-2)$$

$$\left.\frac{I(n\to 2)}{I(3\to 2)}\right|_r : \left.\frac{I(n\to 2)}{I(3\to 2)}\right|_b = (1.000\pm 0.027) + (19\pm 9)\cdot 10^{-3}\cdot (n-3)$$

$$\left.\frac{I(n\to (n-1))}{I(2\to 1)}\right|_r : \left.\frac{I(n\to (n-1))}{I(2\to 1)}\right|_b = (1.000\pm 0.024) + (36\pm 12)\cdot 10^{-3}\cdot (n-2)$$

From this representation a structure effect may also be deduced for the selenium modifications. Although the errors are considerably larger than in the case of phosphorus, the trend remains the same. The Paschen and Brackett series ratios are more or less compatible with unity. Of special interest are the intensity ratios in the Paschen series as there were indications of a pronounced structure effect from an older measurement [10].

$$\left.\frac{I(5\to 3)}{I(4\to 3)}\right|_r : \left.\frac{I(5\to 3)}{I(4\to 3)}\right|_b = \begin{cases} 0.986\pm 0.019 & \text{present work} \\ 0.74\ \ \pm 0.06 & \text{Tauscher et al. [10]} \end{cases}$$

Our data do not sustain the earlier results, but are in agreement with the results obtained from pionic data by the same authors [10] for the above transitions.

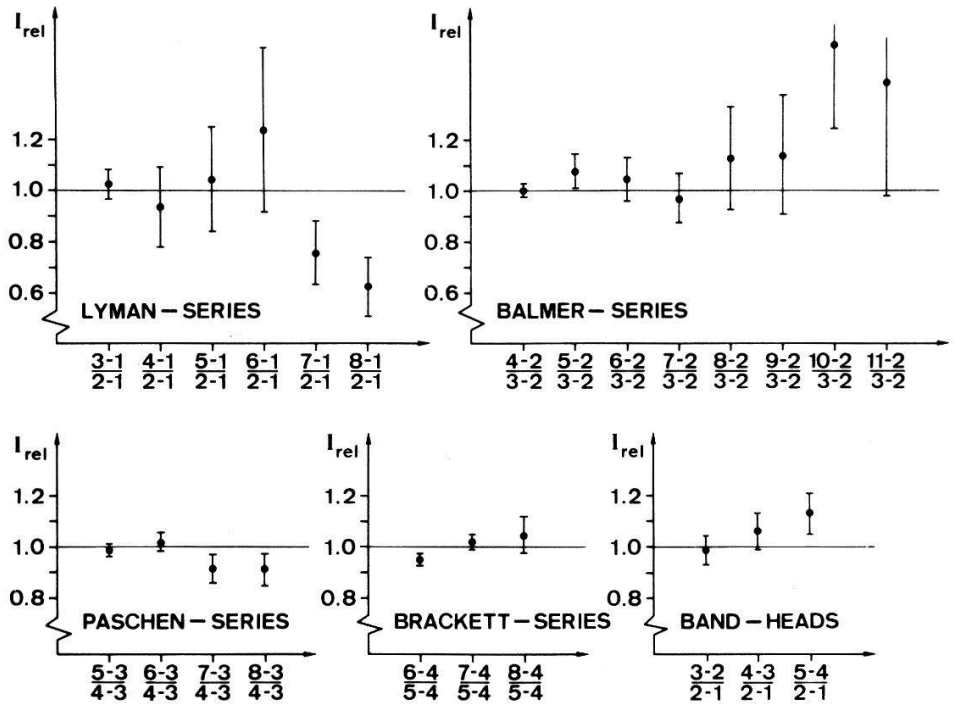

Figure 5
Relative muonic intensity ratios of red to black selenium.

The measured cascade intensities are best reproduced with a parameter

$\alpha = -0.045 \pm 0.018$ ($\chi^2 = 5.66$) for red selenium and with a value of

$\alpha = -0.042 \pm 0.017$ ($\chi^2 = 7.80$) for black selenium.

5.4. *Lyman series limits*

The intensity spectrum of the Lyman series (Fig. 6) can give information on the Coulomb capture mechanism of the muon. Open questions are e.g.:

- What is the main quantum number of the atomic level into which the muon is captured, or:
- Do molecular muonic orbits exist?

Using a classical model [31] one can estimate the highest possible atomic state n_{max}. This state is determined by the interatomic distance between nearest neighbours. For neighbouring atoms with the same charge number z one finds, neglecting electron screening effect,

$$n_{max} = \tfrac{1}{2} \cdot (z \cdot x)^{1/2},$$

where x is the interatomic distance in units of the muonic Bohr radius in hydrogen. Using the interatomic distances given in Section 2.1 and Section 2.2, one obtains for phosphorus a maximum main quantum number $n_{max} \approx 57$ and for selenium $n_{max} \approx 88$.

On the other hand, the energies of muonic transitions from hypothetical molecular states to the $1s$ state are only insignificantly smaller than the $1s$ binding energy. The high energy end of the Lyman series allows therefore an estimate of an upper limit of radiative intensities from molecular states directly to the $1s$ state. For this purpose, we have calculated the energy of an $\infty \rightarrow 1$ transition

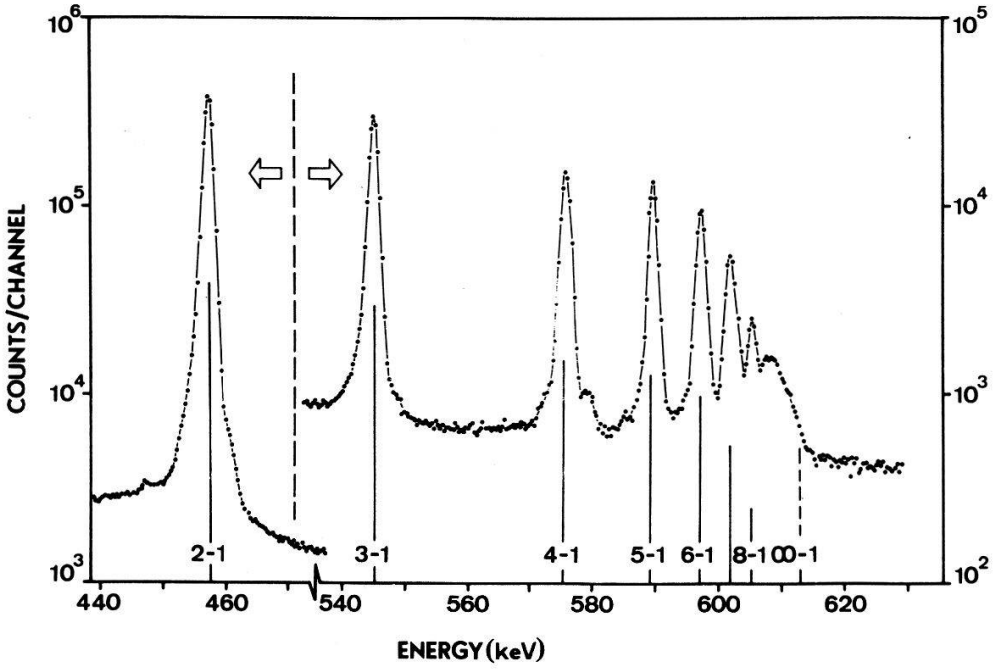

Figure 6
Part of the prompt spectrum of the 50 cm³ Ge(Li) diode: Lyman series of white phosphorus.

Table 6
Intensity limits for molecular transitions

	$E(1s)_{calc}$ keV	$V_{0screen}$ keV	$E(1s)$ keV	Intensity %
μ^-P:	614.4	1.485	612.9	<0.045
μ^-Se:	2770.96	4.942	2766.02	<0.35

taking into account the electron screening [32]. We assumed that the highest atomic transition is the $14 \rightarrow 1$ transition. We then fitted the intensity above background at the position of the $\infty \rightarrow 1$ transition assuming the same line shape and width as for the higher Lyman series transitions. The obtained lower limits for radiative molecular transitions are given in Table 6.

6. Discussion

The experimental results on muonic cascade intensities in phosphorus and selenium demonstrate that the solid state structure influences the atomic capture mechanism of a muon and (or) its subsequent cascade. Because of statistics, such an effect is more pronounced between two allotropic modifications of phosphorus than in selenium.

Specifically, we have observed differences in the Lyman series intensities between the amorphous modifications (white phosphorus, red selenium) and the metallic modifications (black phosphorus, black selenium). The differences have the same trend for both elements and are of comparable magnitude. Between the red (polymer) modification of phosphorus and the black one, no structure effects have been observed.

Cascade calculations show that the Lyman series intensities are most sensitive to differences in the initial distribution over angular momentum states. The Lyman intensities are therefore expected to be most strongly influenced by solid state modifications. In higher series (Balmer, Paschen etc.) the differences are less pronounced.

In trying to explain the observed effects, the bond structures of the various modifications have to be considered. The number of valence electrons participating in the interatomic covalent bonds of an element is the same in all modifications. However, there are differences in the strengths of the Van der Waal's bond between the atomic structures. A loose cohesion of the atomic structures as in the amorphous modifications indicates a weak intermolecular bond, whereas a well structured crystal lattice indicates a strong intermolecular bond. Since the Van der Waal's bonds are produced by those valence electrons which do not take part in the interatomic covalent bond, the number of free valence electrons diminishes with increasing crystallinity. The present experimental results suggest a correlation between the number of free valence electrons and the relative muonic intensities in the Lyman series. In the amorphous modifications the Lyman series intensity ratios are smaller than in the crystalline modifications where there are less free valence electrons. A similar effect has been found in the relative

intensities of the Lyman series in chlorine in NaCl and $NaClO_4$, in sulphur in CaS and $CaSO_4$ [7] and in nitrogen in BN, $NaNO_2$ and $NaNO_3$ [6].

Considering the present results, a remeasurement of the diamond and graphite modifications of carbon and boron nitride becomes of renewed interest. The statistical uncertainties in the recent measurements of Knight et al. [12] are too high to show possible structure effects. Such an experiment should again be performed with high statistics, better detector resolution and with special attention to the higher transitions in the Lyman series.

The authors wish to thank Prof. O. Huber for his continuous interest in this work. They appreciate the hospitality of the SIN staff members and the support of the SIN accelerator crew.

LITERATUR

[1] H. SCHNEUWLY, in "*Exotic Atoms*" ed. by G. FIORENTINI and G. TORELLI, INFN Press (1977), p. 255.
[2] C. E. WIEGAND and G. L. GODFREY, Phys. Rev. *A9*, 2282 (1974).
[3] G. T. CONDO, Phys. Rev. Lett. *33*, 126 (1974).
[4] G. L. GODFREY and C. E. WIEGAND, Phys. Lett. *56B*, 255 (1975).
[5] R. KUNSELMAN, J. LAW, M. LEON and J. MILLER, Phys. Rev. Lett. *36*, 446 (1976).
[6] T. DUBLER, K. KAESER, B. ROBERT-TISSOT, L. A. SCHALLER, L. SCHELLENBERG and H. SCHNEUWLY, Phys. Lett. *57A*, 325 (1976).
[7] L. F. MAUSNER, R. A. NAUMANN, J. A. MONARD and S. N. KAPLAN, Phys. Rev. *A15*, 479 (1977).
[8] L. F. MAUSNER, R. A. NAUMANN, J. A. MONARD and S. N. KAPLAN, Phys. Lett. *56B*, 145 (1975).
[9] H. SCHNEUWLY, T. DUBLER, K. KAESER, B. ROBERT-TISSOT, L. A. SCHALLER and L. SCHELLENBERG, Phys. Lett. *66A*, 188 (1978).
[10] L. TAUSCHER, G. BACKENSTOSS, S. CHARALAMBUS, H. DANIEL, H. KOCH, G. POELZ and H. SCHMITT, Phys. Lett. *27A*, 581 (1968).
[11] T. DUBLER, K. KAESER, B. ROBERT-TISSOT, L. A. SCHALLER, L. SCHELLENBERG and H. SCHNEUWLY, in "*Mesons in Matter*" (Proceedings of the Int. Symposium of Meson Chemistry and Mesomolecular Processes in Matter, Dubna, 7–10 June, (1977) JINR-10908, p. 146.
[12] J. D. KNIGHT, C. J. ORTH, M. E. SCHILLACI, R. A. NAUMANN, H. DANIEL, K. SPRINGER and H. B. KNOWLES, Phys. Rev. *A13*, 43 (1976).
[13] V. G. ZINOV, A. K. KATCHALKIN, L. N. NIKITJUK, V. N. PROKROVSKY, V. N. RIBAKOV and I. A. YUTLANDOV, in "*Mesons in Matter*", (1977) JINR-10908, Dubna, p. 150.
[14] Nouveau Traité de Chimie Minérale $\bar{X}$, (1956) 740, Masson, Paris.
[15] H. KREBS, Z. Anorg. Allg. Chemie *266*, 175 (1951).
[16] H. KREBS and T. LUDWIG, Z. Anorg. Chemie *294*, 257 (1958).
[17] H. KREBS, H. WEITZ and K. H. WORMS, Z. Anorg. Allg. Chemie *280*, 119 (1955).
[18] H. KREBS, Angew. Chemie *70*, 615 (1958).
[19] M. L. HUGGINS, J. Chem. Physics *13*, 37 (1945).
[20] G. BRAUER, Hdbuch der Präp. Anorg. Chemie *1*, 469 (1060).
[21] T. DUBLER, K. KAESER, B. ROBERT-TISSOT, L. A. SCHALLER, L. SCHELLENBERG and H. SCHNEUWLY, Nucl. Phys. *A294*, 397 (1978).
[22] H. BACKE, R. ENGFER , U. JAHNKE, E. KANKELEIT, R. M. PEARCE, C. PETITJEAN, L. SCHELLENBERG, H. SCHNEUWLY, W. U. SCHROEDER, H. K. WALTER and A. ZEHNDER, *Nucl. Phys. A189*, 472 (1972).
[23] B. ROBERT-TISSOT, Thèse No. 743, Université de Fribourg, 1975.
[24] E. STORM and H. I. ISRAEL, Atomic Data and and Nucl. Tables *7*, 565 (1970).
[25] P. WINIGER, O. HUBER and J. HALTER, in "*Rapid Methods for Measuring Radioactivity in the Environment*", IAEA-SM 148/76 (1971).
[26] R. BERGMANN, H. DANIEL, F. J. HARTMANN, J. J. REIDY and W. WILHELM, in "*Mesons in Matter*" (1977) 156, *JINR*-10908, Dubna.
[27] G. A. RINKER, Comput. Phys. Commun. *16*, 221 (1979).
[28] L. A. SCHALLER, T. DUBLER, K. KAESER, G. A. RINKER, B. ROBERT-TISSOT, L. SCHELLENBERG and H. SCHNEUWLY, Nucl. Phys. *A304*, 225 (1978).

[29] J. HUEFNER, Z. Physik *195*, 365 (1966). Programm "CASC1", modified by T DUBLER, K. KAESER and H. SCHNEUWLY.
[30] V. R. AKYLAS and P. VOGEL, Comput. Phys. Commun. *15*, 291 (1978).
[31] L. I. PONOMAREV, Ann. Rev. Nucl. Sci. *23*, 359 (1973).
[32] P. VOGEL, Atomic Data and Nucl. Data Tables *14*, 599 (1974).
[33] R. A. FERRELL, Phys. Rev. Lett. *4*, 425 (1960).